

Prognostic Impact of Vitamin B6 Metabolism in Lung Cancer

Lorenzo Galluzzi,^{1,2,3,40} Ilio Vitale,^{1,2,3,40} Laura Senovilla,^{1,2,3,40} Ken André Olausson,^{2,3,4} Guillaume Pinna,^{5,6} Tobias Eisenberg,⁷ Aïcha Goubar,^{2,3,4} Isabelle Martins,^{1,2,3} Judith Michels,^{1,2,3} Gueorgui Kratassiouk,^{5,6} Didac Carmona-Gutierrez,⁷ Marie Scoazec,^{2,8} Erika Vacchelli,^{1,2,3} Frederic Schlemmer,^{1,2,3} Oliver Kepp,^{1,2,3} Shensi Shen,^{1,2,3} Maximilien Tailler,^{1,2,3} Mireia Niso-Santano,^{1,2,3} Eugenia Morselli,^{1,2,3} Alfredo Criollo,^{1,2,3} Sandy Adjemian,^{1,2,3} Mohamed Jemaà,^{1,2,3} Kariman Chaba,^{2,9,14} Claire Pailleret,^{1,2,3} Mickaël Michaud,^{1,2,3} Federico Pietrocola,^{1,2,3} Nicolas Tajeddine,^{1,2,3} Thibault de La Motte Rouge,¹⁵ Natalia Araujo,^{5,6} Nadya Morozova,^{5,6} Thomas Robert,^{2,10} Hugues Ripoche,^{2,16} Frederic Commo,^{2,3,4} Benjamin Besse,^{2,11} Pierre Validire,¹⁷ Pierre Fouret,^{18,19,20} Angélique Robin,^{2,3,4} Nicolas Dorvault,^{2,3,4} Philippe Girard,²¹ Sébastien Gouy,¹² Patricia Pautier,¹¹ Nora Jägemann,²² Ann-Christin Nickel,²³ Sabrina Marsili,²⁴ Caroline Paccard,^{25,26,27} Nicolas Servant,^{25,26,27} Philippe Hupé,^{25,26,27,28} Carmen Behrens,²⁹ Parviz Behnam-Motlagh,³⁰ Kimitoshi Kohno,³¹ Isabelle Cremer,³² Diane Damotte,³³ Marco Alifano,³⁴ Øivind Midttun,³⁵ Per Magne Ueland,³⁶ Vladimir Lazar,^{2,10} Philippe Dessen,^{2,10,18} Hans Zischka,²² Etienne Chatelut,²⁴ Maria Castedo,^{1,2,3} Frank Madeo,⁷ Emmanuel Barillot,^{25,26,27} Juergen Thomale,²³ Ignacio Ivan Wistuba,²⁹ Catherine Sautès-Fridman,^{32,37,38} Laurence Zitvogel,^{2,9,14} Jean-Charles Soria,^{2,3,4,13} Annick Harel-Bellan,^{5,6} and Guido Kroemer^{1,8,32,37,39,*}

¹INSERM, U848, F-94805 Villejuif, France

²Institut Gustave Roussy, F-94805 Villejuif, France

³Université Paris-Sud XI, F-94805 Villejuif, France

⁴INSERM, U981, F-94805 Villejuif, France

⁵Université Paris-Sud XI, PArI Platform, F-91191 Gif-sur-Yvette, France

⁶CNRS, FRE3377, F-91191 Gif-sur-Yvette, France

⁷Institute of Molecular Biosciences, University of Graz, A-8010 Graz, Austria

⁸Metabolomics Platform

⁹Center of Clinical Investigations in Biotherapies of Cancer (CICBT 507)

¹⁰Unité de Génomique Fonctionnelle et Bioinformatique

¹¹Department of Medical Oncology

¹²Department of Surgery

¹³SITEP (Phase I Unit)

Institut Gustave Roussy, F-94805 Villejuif, France

¹⁴INSERM, U1015, F-94805 Villejuif, France

¹⁵Service d'Oncologie Médicale, Groupe Hospitalier Pitié-Salpêtrière, F-75651 Paris, France

¹⁶CNRS, UMR8200, F-94805 Villejuif, France

¹⁷Service d'Anatomie Pathologique, Institut Mutualiste Montsouris, F-75014 Paris, France

¹⁸INSERM, U985, F-94805 Villejuif, France

¹⁹Service d'Anatomie Pathologique, Groupe Hospitalier Pitié-Salpêtrière, F-75651 Paris, France

²⁰Université Pierre et Marie Curie VI, F-75005 Paris, France

²¹Département Thoracique, Institut Mutualiste Montsouris, F-75014 Paris, France

²²Institute of Toxicology, Helmholtz Center Munich, German Research Center for Environmental Health, D-85764 Neuherberg, Germany

²³Institute for Cell Biology (Cancer Research), University of Duisburg-Essen Medical School, D-45122 Essen, Germany

²⁴EA4553 Institut Claudius-Regaud, F-31052 Toulouse, France

²⁵Institut Curie, F-75248 Paris, France

²⁶INSERM, U900, F-75248 Paris, France

²⁷Mines ParisTech, F-77300 Fontainebleau, France

²⁸CNRS, UMR144, F-75248 Paris, France

²⁹The University of Texas MD Anderson Cancer Center, Houston, TX 77030, USA

³⁰Department of Medical Biosciences, Umeå University, SE-901 87 Umeå, Sweden

³¹Department of Molecular Biology, School of Medicine, University of Occupational and Environmental Health, 807-8555 Kitakyushu, Japan

³²Centre de Recherche des Cordeliers, F-75006 Paris, France

³³Pathology Département, Université Paris Descartes V, F-75270 Paris, France

³⁴Thoracic Surgery Department, Hôtel Dieu, APHP, F-75004 Paris, France

³⁵Bevital AS, N-5021 Bergen, Norway

³⁶Section for Pharmacology, Institute of Medicine, University of Bergen, N-5021 Bergen, Norway

³⁷Université Paris Descartes V, F-75270 Paris, France

³⁸INSERM, U872, F-75006 Paris, France

³⁹Pôle de Biologie, Hôpital Européen Georges Pompidou, AP-HP, F-75908 Paris, France

⁴⁰These authors contributed equally to this work

*Correspondence: kroemer@orange.fr

<http://dx.doi.org/10.1016/j.celrep.2012.06.017>

SUMMARY

Patients with non-small cell lung cancer (NSCLC) are routinely treated with cytotoxic agents such as cisplatin. Through a genome-wide siRNA-based screen, we identified vitamin B6 metabolism as a central regulator of cisplatin responses *in vitro* and *in vivo*. By aggravating a bioenergetic catastrophe that involves the depletion of intracellular glutathione, vitamin B6 exacerbates cisplatin-mediated DNA damage, thus sensitizing a large panel of cancer cell lines to apoptosis. Moreover, vitamin B6 sensitizes cancer cells to apoptosis induction by distinct types of physical and chemical stress, including multiple chemotherapeutics. This effect requires pyridoxal kinase (PDXK), the enzyme that generates the bioactive form of vitamin B6. In line with a general role of vitamin B6 in stress responses, low PDXK expression levels were found to be associated with poor disease outcome in two independent cohorts of patients with NSCLC. These results indicate that PDXK expression levels constitute a biomarker for risk stratification among patients with NSCLC.

INTRODUCTION

During the past two decades, major efforts have been dedicated to the mechanistic exploration of biochemical and metabolic features that constitute common denominators of neoplasia, irrespective of its histologic origin. According to the milestone conceptualization by Hanahan and Weinberg, such hallmarks of cancer include an elevated resistance to the induction of cell death (Hanahan and Weinberg, 2000, 2011). Thus, cancer cells fail to die in response to signals that would lead to the demise of normal cells, a feature that sustains early oncogenesis (when cancer cells become able to tolerate the stress caused by oncogene activation), tumor progression (when cancer cells endure harsh environmental conditions, such as those encountered within poorly vascularized tumor nodules) and resistance to radiation therapy and chemotherapy (which, in principle, aim at activating cell-intrinsic pathways to cell death) (Hanahan and Weinberg, 2000, 2011).

Cell death resistance can result from the inactivation/downregulation of positive modulators of apoptosis, like TP53 and ARF (Brown et al., 2009; Gil and Peters, 2006), or the hyperactivation/overexpression of anti-apoptotic factors such as BCL-2-like and inhibitor of apoptosis proteins (Gyrd-Hansen and Meier, 2010; Youle and Strasser, 2008). Moreover, malignant cells can acquire resistance to otherwise lethal conditions in the context of (and sometimes due to) an extensive rewiring of metabolic circuitries (Kroemer and Pouyssegur, 2008; Ward and Thompson, 2012). For instance, the pentose phosphate pathway is often hyperactivated in cancer cells, supplying them with anabolic substrates as well as with reducing equivalents that can be used to counteract oxidative stress (Anastasiou et al.,

2011). Accumulating evidence indicates that the molecular cascades that regulate cell death and metabolism are extensively intertwined (Buchakjian and Kornbluth, 2010; Vousden and Ryan, 2009). Thus, one of the major checkpoints of cell death regulation, i.e., mitochondrial membrane permeabilization, is profoundly influenced by bioenergetic metabolism (Alavian et al., 2011; Kroemer et al., 2007), and the expression profile of pro-apoptotic BH3-only proteins as well as metabolic biomarkers have been shown to predict the fate of patients with cancer (Lodi and Ronen, 2011; Ni Chonghaile et al., 2011).

Paradoxically, current anticancer therapies aim at killing malignant cells that, in the majority of cases, are intrinsically resistant to the induction of cell death, at least to some extent. Even when an initial pyrrhic response to therapy can be attained, leading to a transient reduction in the tumor burden, the Darwinian selection of chemoresistant clones often determines chemotherapeutic failure (Sève and Dumontet, 2005). As a standalone example, non-small cell lung cancer (NSCLC), one of the leading causes of cancer-related death among males (Jemal et al., 2008), is frequently treated with platinum derivatives such as cisplatin (cis-diammineplatinum(II) dichloride, CDDP), yielding highly heterogeneous and, in the best-case scenario, transitory responses (Cosaert and Quoix, 2002).

On the basis of these premises and incognita, we decided to launch a genome-wide siRNA screen to identify novel proteins that affect the response of NSCLC to CDDP. Here, we report 85 newly identified CDDP response modifiers (CRMs), including pyridoxal kinase (PDXK), the enzyme that generates the biologically active form of vitamin B6. Furthermore, we demonstrate that the vitamin B6 precursor pyridoxine (PN) exacerbates, in a PDXK-dependent fashion, CDDP cytotoxicity *in vitro* and *in vivo*, as well as the response of cancer cells to CDDP-unrelated stress conditions. Finally, we show that the expression levels of PDXK influence the fate of patients with cancer, suggesting that PDXK may constitute a novel prognostic biomarker for risk stratification.

RESULTS

Genome-wide siRNA Screen for the Identification of CRMs

To identify novel factors involved in the cellular response to CDDP, we transfected human NSCLC A549 cells with a panel of small interfering RNAs covering the entire genome (two siRNAs targeting a total of 23,078 gene products) and then exposed them to 50 μ M CDDP for 24 hr. These conditions were selected as they led to the death of ~50% of cells that had been transfected with a control siRNA. At the end of the assay, cytotoxicity and cell number were estimated by measuring the release of lactate dehydrogenase (LDH) into the cell supernatant and the conversion of a tetrazolium salt (WST-1), respectively. At this stage, 12.6% of all siRNAs were excluded from further analyses, as they exerted per se (in the absence of CDDP) cytotoxic or antiproliferative effects. Conversely, gene products for which both siRNAs modulated the cellular response to CDDP in a concordant fashion (i.e., they both reduced or they both exacerbated CDDP cytotoxicity) were ranked based on their biological potency, and the top 1,000

ones were subjected to a first round of validation. This round, which entailed two additional siRNAs per gene product, allowed us to identify 85 gene products whose downregulation by at least three out of four non-overlapping siRNAs concordantly modulated the response of A549 cells to CDDP (Figure 1A and Table S1). Fifty-three of these hits were “cytoprotectors” (their depletion enhanced CDDP cytotoxicity) while 32 were “chemosensitizers” (their knockdown inhibited CDDP cytotoxicity), and at least 34 among them (24 cytoprotectors and eight chemosensitizers) were “druggable” (at least in vitro) according to the current knowledge (Figure S1A). Chemosensitizers included the anaplastic lymphoma kinase (ALK), a receptor tyrosine kinase that is frequently involved in oncogenic fusion proteins (i.e., NPM-ALK) (Morris et al., 1994). While previous reports indicate that wild-type ALK is not expressed by NSCLC cells (Iwahara et al., 1997; Morris et al., 1994; Rikova et al., 2007; Stoica et al., 2002), we validated our finding by immunoblotting, upon transfection of A549 cells with a control siRNA or with two, nonoverlapping siRNAs targeting ALK (data not shown).

To validate the screening results, A549 cells were subjected to the siRNA-mediated knockdown of selected druggable hits and then exposed to sub-apoptotic (25 μ M) or highly cytotoxic (75 μ M) doses of CDDP (which are best suited to highlight chemosensitization and cytoprotection, respectively) for 48 hr, and then assayed by cytofluorometry for cell death-related parameters (i.e., dissipation of the mitochondrial transmembrane potential and plasma membrane breakdown) (Figures S1B and S1C and Table S2). As a complementary validation, cells were incubated with CDDP alone or in the presence of specific pharmacologic inhibitors of druggable hits (Figure S1D). In line with the results of the primary screen, both the depletion and inhibition of ZDHHC9 (a palmitoyl transferase of H-RAS and N-RAS), interleukin 6 (IL6) or its receptor (IL6R), BCL2L1 (better known as BCL-X_L), and RAC2 (a small GTP-binding protein) sensitized A549 cells to CDDP-induced cell death, while the depletion/inhibition of two distinct cytochrome c oxidase (COX) subunits and that of apoptotic peptidase activating factor 1 (APAF1) exerted cytoprotective effects (Figures S1B–S1D). Thus, our screen identified known modulators of apoptosis (such as BCL-X_L and APAF1) as well as proteins that had never been implicated in CDDP-elicited signaling pathways.

Identification of General Cell Death Modulators versus CRMs

To discriminate between general regulators of cell death and specific CRMs, we assessed our 85 hits (1) for their capacity to modulate CDDP cytotoxicity in six distinct CDDP-resistant A549 clones, four additional NSCLC cell lines, four ovarian carcinoma cell lines, and wild-type or *TP53*^{-/-} HCT 116 colon cancer cells (Figure 1A); and (2) for their capacity to influence the response of A549 cells to 13 different cytotoxic agents including three platinum compounds (CDDP, carboplatin, and oxaliplatin), six platinum-unrelated anticancer drugs (betulinic acid, camptothecin, doxorubicin, etoposide, mitoxantrone, and mytomicin c), and four cellular toxins (ceramide, cadmium, staurosporine, and thapsigargin) (Figure 1B). Unsupervised hierarchical clustering of these data sets revealed the existence of response patterns that were similar in cancer cells of the same type (for instance, all

NSCLC cell lines or ovarian cell lines but TOV-112D) as well as of cell line-specific profiles (such as that of TOV-112D cells) (Figure 1A and Table S3). This method also uncovered the existence of general (e.g., COX5B, PSMD7, TRIP4) and agent-specific (e.g., ALK, CLIC1, IL6R, etc.) modulators of the cell death response (Figure 1B and Table S4). Moreover, we found that the depletion of the 85 hits identified in our screen induced relatively similar modifications in the response of A549 cells to CDDP and carboplatin, yet rather dissimilar changes when CDDP and oxaliplatin were compared (Figure 1B and Table S4). This reflects previously reported differences in the mechanisms of action of these platinum-based chemotherapeutics (Galluzzi et al., 2010; Tesniere et al., 2010).

Combinatorial Screening of CRMs

To gain further insights into the functional connections among the CRMs identified in our screen, we performed a systematic combinatorial analysis. To this aim, we used siRNAs for the depletion of each of our 85 hits as well as of seven additional proteins that we and others had identified as CRMs (BAK1, BAX, BCL2, CASP2, STAT3, TP53, VDAC1) (Castedo et al., 2006; de La Motte Rouge et al., 2007; Seth et al., 2005; Tajeddine et al., 2008). A549 cells were transfected in triplicate instances with 92 \times 92 couples of siRNAs (a total of 25,392 test conditions, controls excluded), treated with CDDP as in the original screen, and assayed for WST-1 conversion. The resultant matrix of combinatorial effects (Figure 2) was subjected to unsupervised hierarchical clustering (following the Ward method and the Pearson correlation), leading to the identification of four separate clusters of functionally noninteracting gene products (Table S5).

Thus, the simultaneous knockdown of hits belonging to the same cluster failed to yield any functional interaction (i.e., the effects of the codepletion were equal to the effects of the depletion of either these two hits alone). Conversely, the concomitant knockdown of hits belonging to distinct clusters caused at least additive effects. Some of these results were expected (such as the classification of the anti-apoptotic proteins BCL2, BCL-X_L, and MCL1 together in cluster 1, that of the COX subunits Vb and VIId together in cluster 3, and that of the pro-apoptotic proteins BAX, BAK1, APAF1, TP53, VDAC1, CASP2, the BCL2 interactor NLRP1, and two proteasome subunits together in cluster 4), while others were not (such as the presence of IL6R, STAT3, and CLIC1 in cluster 1). This approach was validated by using siRNAs (Figures S2A–S2C), pharmacologic inhibitors (Figures S2D–S2F) and cytofluorometry as an alternative readout. The combined depletion/inhibition of ZDHHC9 (which is targeted by 2-bromopalmitate) and IL6R (which can be blocked by an extracellular antibody), both belonging to cluster 1, provided no additional chemosensitization as compared to depletion/inhibition of either these factors alone (Figures S2A and S2D). In contrast, the concomitant knockdown/inhibition of IL6R (in cluster 1) and RAC2 (which can be inhibited by EHT 1864 and belonged to cluster 2) sensitized to CDDP cytotoxicity more than the depletion/inhibition of IL6R or RAC2 alone (Figures S2B and S2E). Along similar lines, the simultaneous downregulation of COX (in cluster 3) and TP53 (in cluster 4) yielded an additional protection against CDDP as compared to the depletion of



Figure 1. Functional Characterization of CRMs in Multiple Cancer Cell Lines and in A549 Cells Challenged with CDDP-Related and -Unrelated Cell Death Inducers

(A) Unsupervised hierarchical clustering of the effects of the 85 hits from the siRNA screen on the response to cisplatin (CDDP) of WT human NSCLC A549 cells, six distinct CDDP-resistant A549 clones (A549 no. 1–6), four NSCLC cell lines other than A549 (i.e., HCC827, H1299, H1650, and H1975 cells), four ovarian cancer cell lines (i.e., A2780, HEY, OV2008, and TOV-112D cells) as well as WT and *TP53*^{-/-} colon carcinoma HCT 116 cells. Green and red boxes depict

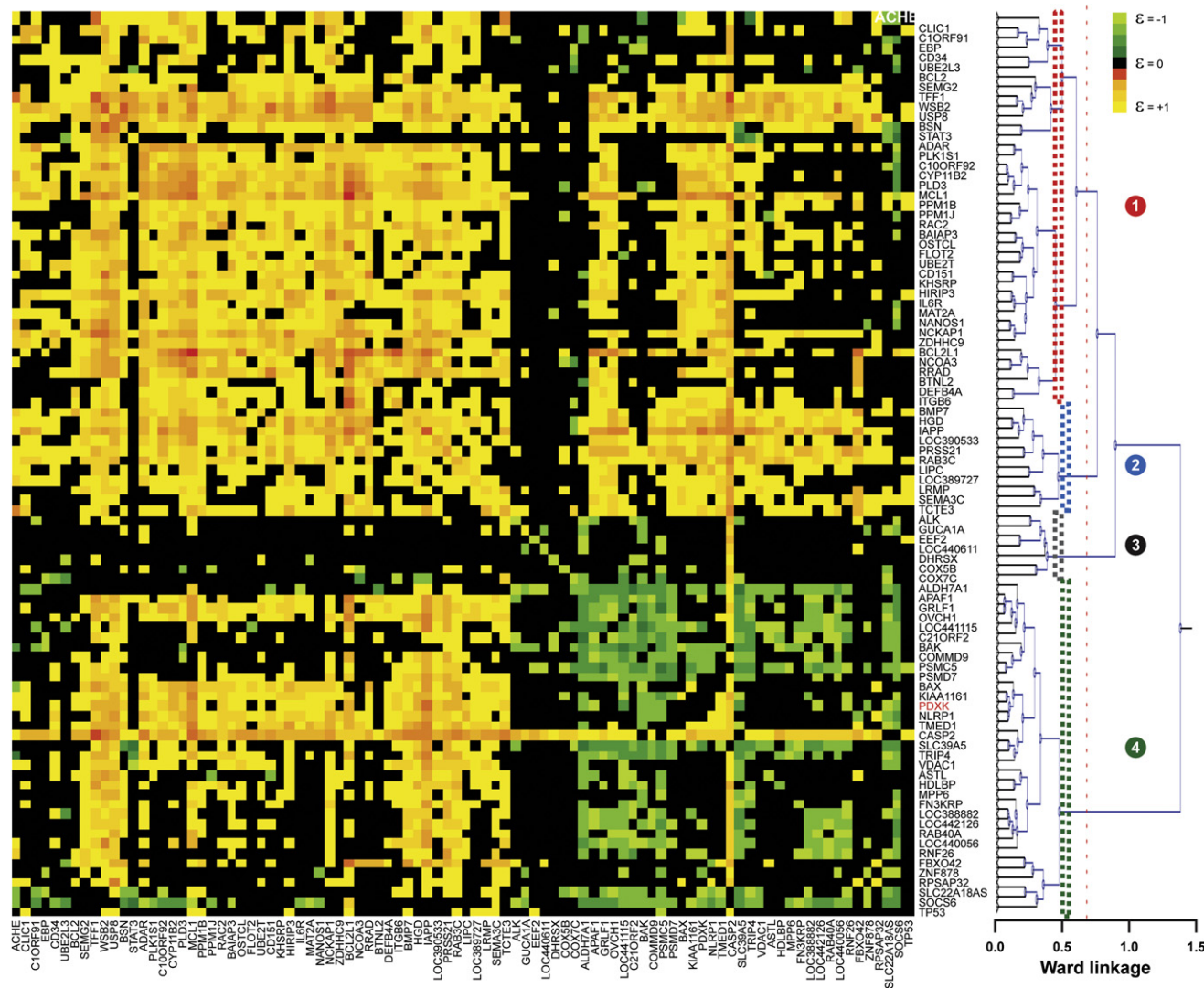


Figure 2. Clustering of the Interactions between CRMs

Clustering of the effects of the co-transfection of each of the 85 hits from the secondary screen (plus 7 control siRNAs) with each other on the response of A549 cells to cisplatin (CDDP). For each couple of siRNAs, colored boxes depict the degree of mutual interaction, ϵ (varying from -1 to $+1$). $\epsilon = 0$ represents the absence of interaction, $\epsilon < 0$ an alleviating interaction (the effects of the cotransfection are lower than the sum of the effects of each siRNA transfected alone), and $\epsilon > 0$ an aggravating interaction (the effects of the cotransfection are higher than the sum of the effects of each siRNA transfected alone). This analysis allows for the identification of four clusters of CDDP response modifiers (CRMs). See also Supplemental Information, Figure S2 and Tables S2 and S5.

either these proteins alone (Figure S2C). Similar results were obtained by inhibiting COX and TP53 with sodium azide and cyclic pifithrin α , respectively (Figure S2F). Altogether, these observations suggest that (at least) four different signaling modules determine CDDP responses.

Impact of Intermediate Metabolism on CDDP Responses, In Vitro and In Vivo

Among the 85 CRMs uncovered by our screen, we were particularly interested in pyridoxal kinase (PDXK), the enzyme that converts vitamin B6 precursors into their bioactive derivative,

siRNA-mediated chemosensitization ($\Delta < 0$) and cytoprotection ($\Delta > 0$), respectively. Δ represents the difference between the residual proliferation (upon the administration of CDDP) in siRNA-transfected cells and the residual proliferation in cells transfected with a control siRNA (siUNR).

(B) Unsupervised hierarchical clustering of the effects of the 85 hits from the siRNA screen on the response of human NSCLC A549 cells to CDDP, betulinic acid, C_2 -ceramide, cadmium chloride, camptothecin, carboplatin, doxorubicin, etoposide, mitoxantrone, mytomyacin C, oxaliplatin, staurosporine, and thapsigargin. Green and red boxes depict siRNA-mediated chemosensitization ($\Delta < 0$) and cytoprotection ($\Delta > 0$), respectively. Δ represents the difference between the residual proliferation (upon the administration of the indicated drug) in siRNA-transfected cells and the residual proliferation in cells transfected with a control siRNA (siUNR). See also Supplemental Information, Figure S1, and Tables S1, S2, S3, and S4.

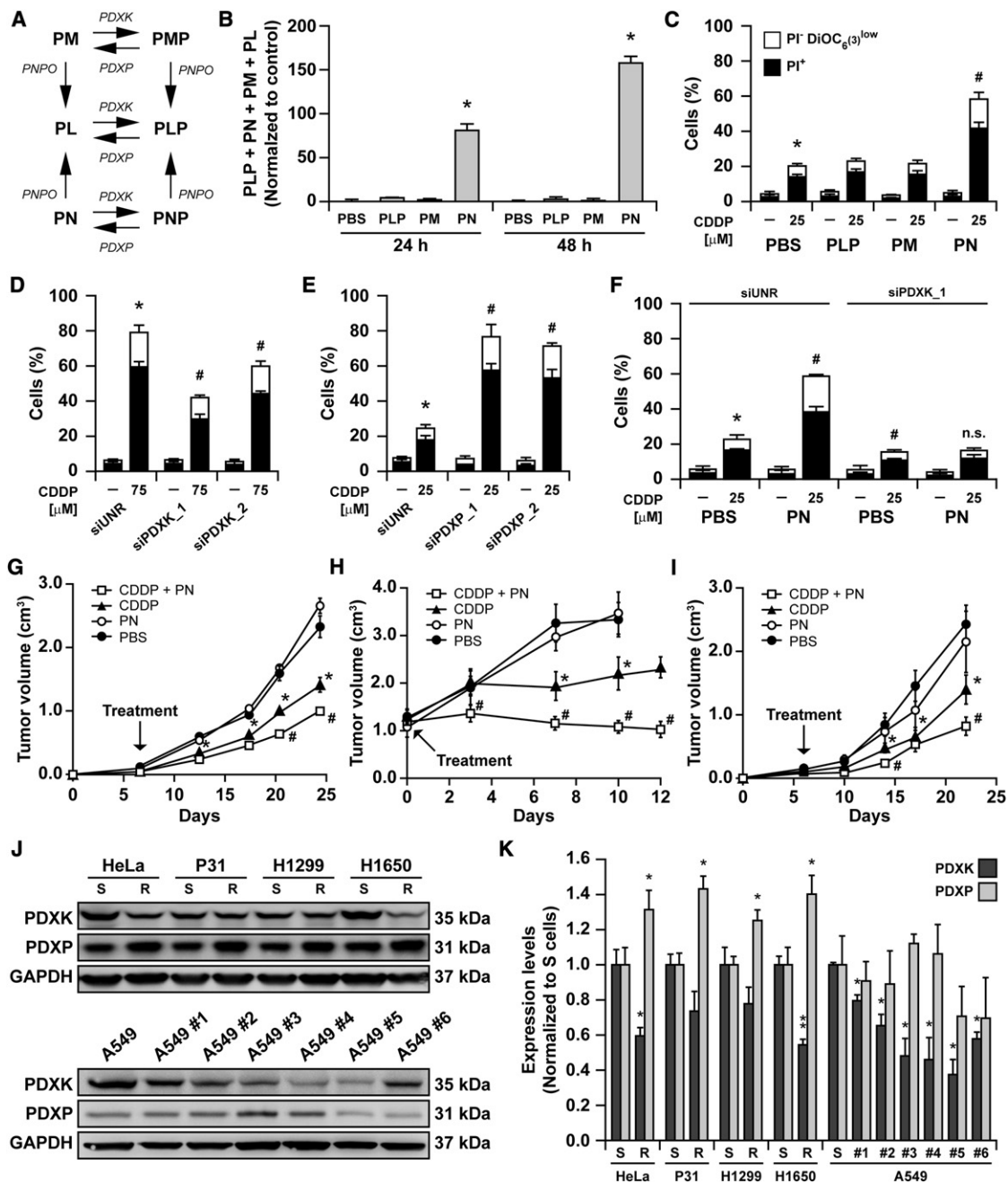


Figure 3. Influence of Vitamin B6 Metabolism on the Response to CDDP of Cancer Cells In Vitro and In Vivo

(A) Schematic representation of vitamin B6 metabolism in humans. PDXK, pyridoxal kinase; PDXP, pyridoxal phosphatase; PNPO, pyridoxamine 5'-phosphate oxidase; PL, pyridoxal; PLP, pyridoxal-5-phosphate; PM, pyridoxamine; PMP, pyridoxamine-5'-phosphate; PN, pyridoxine; PNP, pyridoxine-5'-phosphate.

(B) Quantification of intracellular B6 vitamers (PLP + PN + PM + PL) upon acute administration of PLP, PM or PN to A549 cells for 24 or 48 hr. ** = $p < 0.001$ (Student's *t* test), as compared to PBS-treated cells.

(C) Cytofluorometric assessment of cell death induced by 25 μ M cisplatin (CDDP) in A549 cells co-treated with the indicated B6 vitamers for 48 hr. PI⁺ = dead cells; PI⁻ DiOC₆(3)^{low} = dying cells. Mean \pm SEM ($n = 3$). * = $p < 0.05$ (Student's *t* test), as compared to untreated cells. # = $p < 0.05$ (Student's *t* test), as compared to cells treated with the same concentration of CDDP. See also Figures S3A–S3C and S4.

(D and E) Cytofluorometric assessment of cell death induced by 25 or 75 μ M CDDP in A549 cells transfected with siRNAs targeting the indicated vitamin B6-relevant enzymes. PI⁺ = dead cells; PI⁻ DiOC₆(3)^{low} = dying cells. Mean \pm SEM ($n = 3$). * = $p < 0.05$ (Student's *t* test), as compared to untreated siUNR-transfected cells. # = $p < 0.05$ (Student's *t* test), as compared to siUNR-transfected cells treated with the same concentration of CDDP. See also Figures S3D and S3E.

(F) Combined effects of PDXK depletion and PN administration on CDDP-induced cell death. PI⁺ = dead cells; PI⁻ DiOC₆(3)^{low} = dying cells. Mean \pm SEM ($n = 3$). * = $p < 0.05$ (Student's *t* test), as compared to untreated siUNR-transfected cells. # = $p < 0.05$ (Student's *t* test), as compared to siUNR-transfected cells treated with CDDP only. n.s. = non-significant (Student's *t* test), as compared to siPDXK-transfected cells treated with CDDP only. See also Figure S3D.

pyridoxal-5-phosphate (PLP) (Figure 3A) (Lee et al., 2000), for two reasons. First, the knockdown of PDXK protected all tested cell lines against CDDP cytotoxicity (Figure 1A), and A549 cells against a plethora of cytotoxic agents (Figure 1B), thus far displaying the widest cytoprotective potential in our models. Second, recent results from a large population study demonstrate a negative correlation between vitamin B6 serum levels and the risk of developing NSCLC (Johansson et al., 2010). Thus, we decided to investigate the effect of the bioactive form of vitamin B6 (PLP) and its main precursor pyridoxine (PN) on CDDP responses.

The acute administration of PN (but neither that of PLP, which cannot cross the plasma membrane of most mammalian cells, nor that of pyridoxamine) increased the intracellular concentration of B6 vitamers (Figure 3B) and aggravated CDDP cytotoxicity, as quantified by cytofluorometry (Figure 3C) or by measuring the impedance of viable cells growing on microelectrode-coated plates (Figure S3A). Along similar lines, the continuative presence of higher-than-normal or lower-than-normal amounts of B6 vitamers in the culture medium exacerbated or inhibited, respectively, the response of A549 cells to CDDP (Figure S3B). Moreover, PN aggravated the loss of clonogenic potential triggered in *Saccharomyces cerevisiae* cells by a brief exposure to high doses of CDDP, an effect that was even more pronounced for PLP (Figure S3C). Indeed, PLP is readily taken up by yeast, as demonstrated by the fact that *S. cerevisiae* cells lacking the vitamin B6-related gene *snz1* do not grow in vitamin B6-deficient medium, while they do so upon the addition of PLP (data not shown). Next, we transfected A549 cells with siRNAs targeting PDXK and pyridoxal phosphatase (PDXP), the enzyme that functionally antagonizes PDXK (Figure 3A), and tested their response to CDDP. As expected, PDXK depletion reduced CDDP-induced cell death, while the knockdown of PDXP exacerbated it (Figures 3D, 3E, and S3D). The effects of PN were lost upon PDXK depletion, in line with the notion that PN must be converted into PLP to become biologically active (Figure 3F). In yeast, the knockout of two vitamin B6-related genes, *sno1* and *snz1*, prevented CDDP-induced cell death (Figure S3E).

Systemic injections of PN improved the antitumor effects of CDDP-based chemotherapy in vivo, in murine Lewis lung carcinoma cells transplanted into syngenic C57BL/6 mice, in both models of induction (tumors treated when palpable) and regression (tumors treated when volume reached 1 cm³) (Figures 3G and 3H). The same held true for human NSCLC H460 cells growing in immunodeficient animals (Figure 3I). In vitro, PN exacerbated CDDP cytotoxicity in 8 additional NSCLC cell lines (besides A549 cells), 4 ovarian carcinoma cell lines, cervical carcinoma, osteosarcoma, mesothelioma and wild-type (but not *TP53*^{-/-}) colorectal cancer cells, murine lung carcinoma cells, as well as in multiple distinct CDDP-resistant cell lines

(Figure S4), underscoring the general impact of vitamin B6 metabolism on CDDP responses. Of note, four distinct types of CDDP-resistant cells (as obtained by continuous selection in CDDP-containing medium) exhibited decreased PDXK/PDXP ratio (due to decreased PDXK or increased PDXP protein levels) as compared to their CDDP-sensitive counterparts (Figures 3J and 3K).

Mechanism of Vitamin B6-Mediated Chemosensitization and General Impact of Vitamin B6 Metabolism in Stress Responses

In line with previous reports (Previati et al., 2006), both non-oxidized glutathione (GSH) and *N*-acetylcysteine (NAC) fully prevented apoptosis induction by CDDP (irrespective of the presence of PN) (Figure 4A). Conversely, inhibition of caspases reduced the cytotoxicity of CDDP (alone or in combination with PN), yet it did not completely abrogate PN-mediated chemosensitization (Figure 4A). In the presence of PN, cells treated by a sub-apoptotic concentration of CDDP exhibited increased phosphorylation of TP53 on serines 15 and 46, and increased activation of caspase-3 and -9 (Figure 4B). Moreover, PN significantly increased CDDP-DNA adducts, as quantified by immunofluorescence staining of cells cultured in the presence of CDDP (Figure 4C) followed by automated image analysis (Figure 4D). Accordingly, two signs of an ongoing DNA damage response to CDDP, namely the activating phosphorylation (on Ser 1981) of the ataxia telangiectasia mutated (ATM) kinase and the phosphorylation on Ser 136 of the ATM substrate histone 2AX (H2AX), were aggravated in the presence of PN (Figures 4E–4H). The accumulation of CDDP-DNA adducts as well as the activation of ATM and H2AX were prevented by the presence of NAC in the culture medium. Taken together, these results suggest that PN exacerbates the cytotoxic effects of CDDP (which are mediated by both caspase-dependent and -independent pathways) upstream of the DNA damage response and by a mechanism that can be blocked by antioxidants.

To get further insights into the molecular circuitries underlying vitamin B6-mediated chemosensitization, we performed targeted metabolomic determinations and metabolomic profiling. We found that, in pre-apoptotic conditions, NSCLC cells treated with CDDP and PN exhibited a bioenergetic defect (measured in terms of Atkinson's energy charge = [ATP] + 0.5 [ADP] / [ATP] + [ADP] + [AMP]) (Atkinson, 1968) that was not present in cells incubated with either these compounds alone (Figure 5A and Figures S5A–S5C). Moreover, A549 cells succumbed to CDDP while manifesting a decrease in the intracellular levels of GSH (Figures 5B and 5C) as well as of three metabolites with molecular weights of approximately 161, 203, and 217 Da, which were identified as carnitine, acetyl-carnitine, and propionyl-carnitine, respectively (Figures S5D–S5F). Such a decrease in GSH and redox-relevant metabolites was largely aggravated

(G–I) In vivo growth of murine LLC (G and H) or human NSCLC H460 (I) cells grafted into immunocompetent C57BL/6 (G and H) or immunodeficient Swiss nude (I) mice upon treatment (initiated as indicated) with intraperitoneal CDDP alone or in combination with PN. Mean ± SEM (10–20 mice/group). * = *p* < 0.05 (two-way ANOVA), as compared to PBS-treated mice. # = *p* < 0.05 (two-way ANOVA), as compared to mice treated with CDDP only.

(J and K) PDXK and PDXP expression in isogenic CDDP-sensitive (S) and CDDP-resistant (R) cancer cell lines. Representative immunoblots (J). GAPDH levels were monitored to ensure equal loading of lanes. Quantitative data upon normalization to S cells of the same type (K). Mean ± SEM (*n* = 2–3). * = *p* < 0.05, ** = *p* < 0.001, (Student's *t* test), as compared to S cells of the same type.

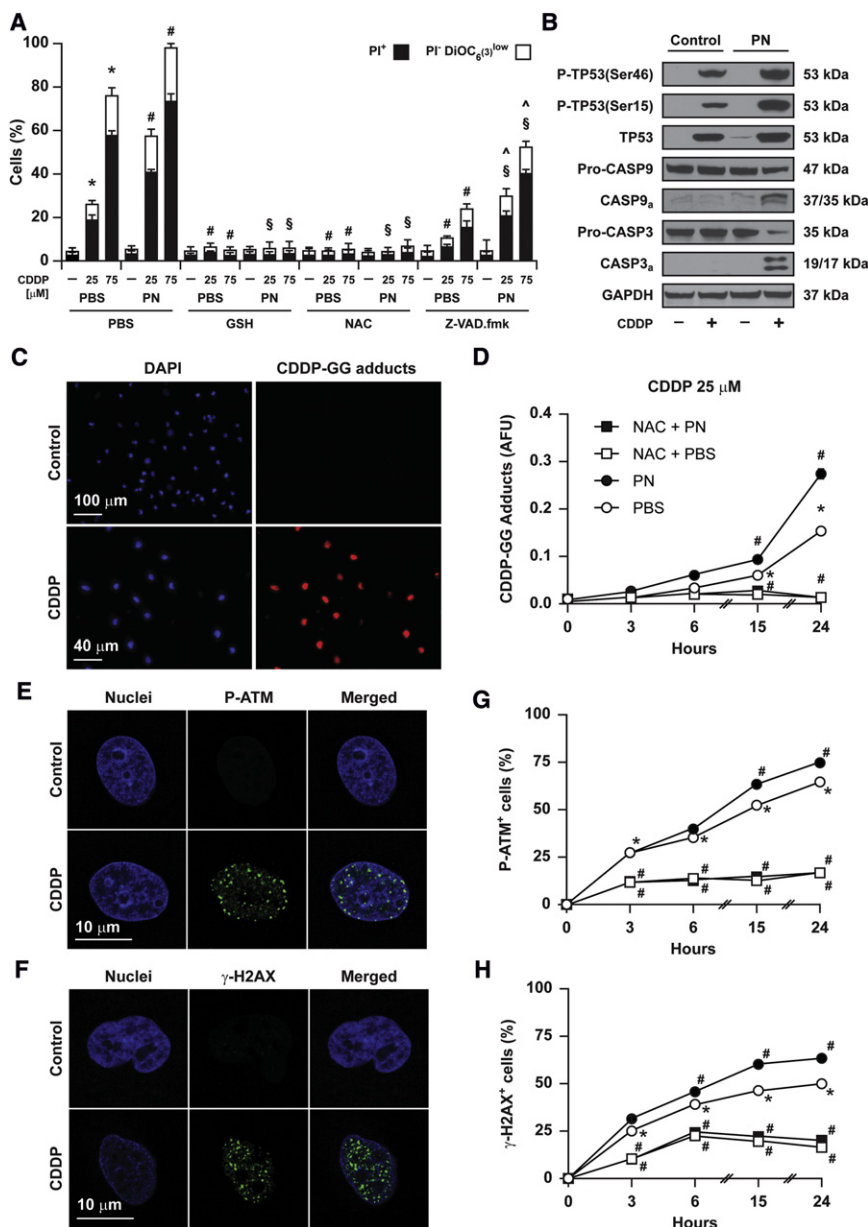


Figure 4. Mechanisms of Chemosensitization by PN In Vitro

(A) Cytofluorometric quantification of A549 cell death induced by 25 or 75 μM cisplatin (CDDP) alone or in combination with pyridoxine (PN) and/or reduced glutathione (GSH), N-acetylcysteine (NAC) and the pan-caspase inhibitor Z-VAD.fmk. PI⁺ = dead cells; PI⁻ DiOC₆(3)^{low} = dying cells. Mean ± SEM (n = 3). * = p < 0.05 (Student's t test), as compared to untreated cells. # = p < 0.05 (Student's t test), as compared to cells treated with the same concentration of CDDP. § = p < 0.05 (Student's t test), as compared to cells treated with the same concentration of CDDP and PN. ^ = p < 0.05 (Student's t test), as compared to cells treated with the same concentration of CDDP and Z-VAD.fmk.

(B) Immunoblotting-based assessment of the activation of the intrinsic apoptosis pathway in A549 cells treated with 25 μM CDDP alone or in combination with PN. CASP, caspase. GAPDH levels were monitored to ensure equal loading.

(C–H) DNA damage response in A549 cells challenged with 25 μM CDDP alone or combined with PN and/or NAC. Representative immunofluorescence microphotographs of CDDP-DNA adducts (C), the activating phosphorylation of ATM (P-ATM) (E) and the phosphorylation of histone 2AX (γ-H2AX) (F) in untreated versus CDDP-treated cells. White bars indicate picture scale (C, E, and F). Kinetic data as obtained upon automatic image analysis of fluorescence (D) or visual quantification of the % of cells exhibiting more than 5 (G) or 10 (H) bright nuclear spots (DNA damage foci). Untreated cells exhibit no CDDP-DNA adducts and baseline (<5% positive cells) activation of the DNA damage response (not shown). Mean ± SEM (n = 3). * = p < 0.05 (Student's t test), as compared to untreated cells. # = p < 0.05 (Student's t test), as compared to cells treated with CDDP only (D, G, and H).

Prognostic Value of PDXK in NSCLC

Given the profound implication of vitamin B6 and PDXK in the response of NSCLC to CDDP as well as in the management of cellular stress, we wanted to investi-

gate the influence of PDXK expression levels in the clinical setting. To this aim, we developed an immunohistochemical staining method that specifically detects PDXK (as demonstrated by the fact that siRNA-mediated depletion of PDXK results in the complete loss of the signal) (Figures S6A and S6B) and applied it to specimens from a first NSCLC patient cohort. These patients were affected by localized NSCLC and underwent surgery followed by optional adjuvant CDDP (Table 1). Upon immunohistochemical analysis (Figure 6A), samples were divided into two groups with high (>median) and low (<median) PDXK expression. High PDXK expression levels had a significant positive impact on both disease-free and overall survival (Figure 6B), independent on whether patients did or did not receive adjuvant chemotherapy (not shown). A similar positive impact of

by PN (Figures 5B, 5C and S5D–S5F). Still, only GSH (Figure 4A) (but not carnitine metabolites, Figures S5G and S5H) could protect cells against the cytotoxic effect of CDDP plus PN. These results indicate that vitamin B6 exerts chemosensitizing effects by interfering in a multipronged fashion with the redox metabolism.

We therefore hypothesized that the vitamin B6 metabolism might have a general impact on the cellular management of stress. Indeed, PN rendered A549 cells more sensitive to hyperthermia, ionizing irradiation, hypoxia, respiratory chain inhibition (with high doses of KCN), and nutrient depletion (Figure 5D). As in the case of CDDP (Figure 3F), PN-mediated sensitization was abrogated by the siRNA-mediated knockdown of PDXK (Figures 5D and S3D).

gated the influence of PDXK expression levels in the clinical setting. To this aim, we developed an immunohistochemical staining method that specifically detects PDXK (as demonstrated by the fact that siRNA-mediated depletion of PDXK results in the complete loss of the signal) (Figures S6A and S6B) and applied it to specimens from a first NSCLC patient cohort. These patients were affected by localized NSCLC and underwent surgery followed by optional adjuvant CDDP (Table 1). Upon immunohistochemical analysis (Figure 6A), samples were divided into two groups with high (>median) and low (<median) PDXK expression. High PDXK expression levels had a significant positive impact on both disease-free and overall survival (Figure 6B), independent on whether patients did or did not receive adjuvant chemotherapy (not shown). A similar positive impact of

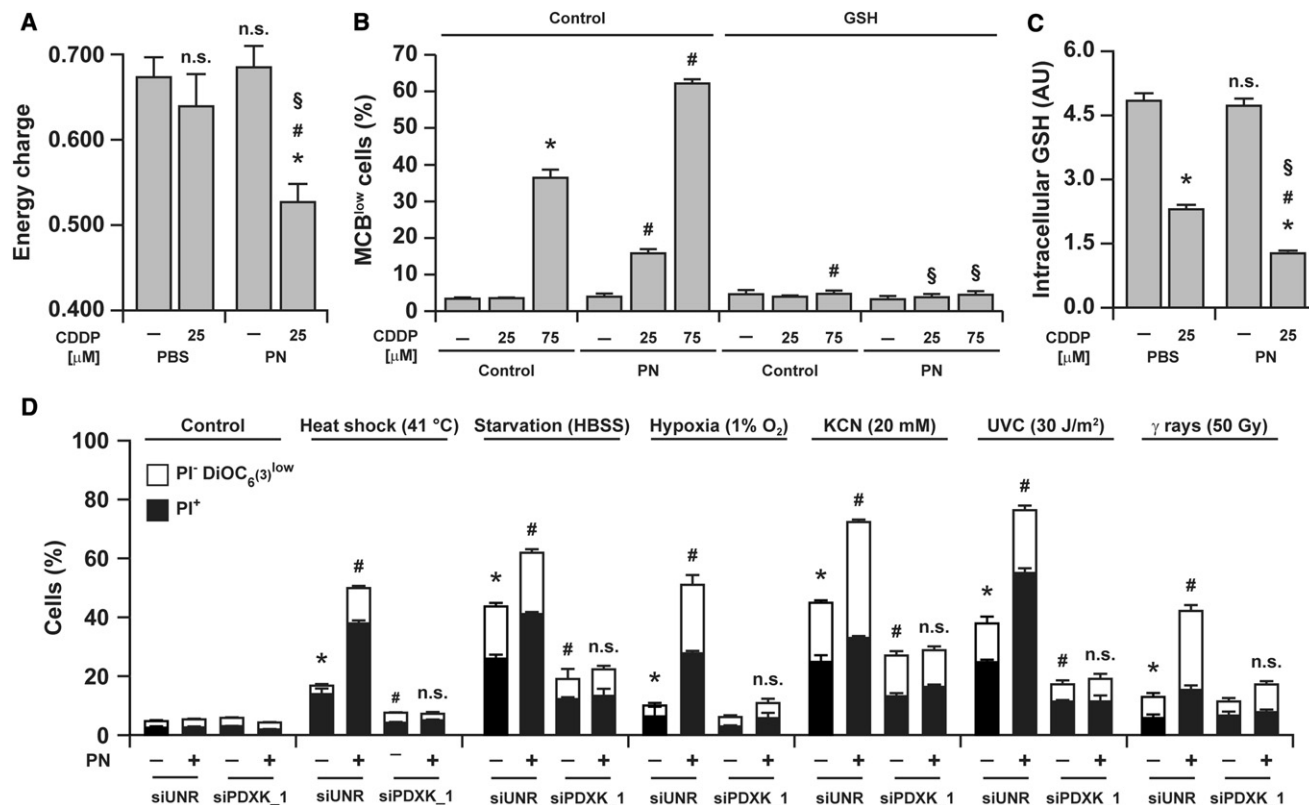


Figure 5. Bioenergetic Aspects of PN-Mediated Chemosensitization and Impact of Vitamin B6 Metabolism in Stress-Induced Cell Death

(A) Atkinson's energy charge of A549 cells treated for 24 hr with 25 μ M cisplatin (CDDP) and pyridoxine (PN), alone or in combination. Mean \pm SEM (n = 6). * = $p < 0.05$ and n.s. = non-significant (Student's t test), as compared to untreated cells. # = $p < 0.05$ (Student's t test), as compared to cells treated with CDDP only. § = $p < 0.05$ (Student's t test), as compared to cells treated with PN only. See also Figures S5A–S5C.

(B) Cytofluorometric assessment of intracellular GSH levels in A549 cells treated for 24 hr with the indicated concentration of CDDP, alone or in combination with PN. Columns report the % of cells with low intracellular GSH (MCB^{low}). Mean \pm SEM (n = 6). * = $p < 0.05$ (Student's t test), as compared to untreated cells. # = $p < 0.05$ (Student's t test), as compared to cells treated with the same concentration of CDDP plus PN. Mean \pm SEM (n = 6). See also Figures S5D–S5H.

(C) Intracellular levels of GSH, as measured by mass spectrometry, in A549 cells treated for 24 hr with 25 μ M CDDP and PN, alone or in combination. Mean \pm SEM (n = 6). * = $p < 0.05$ and n.s. = non-significant (Student's t test), as compared to untreated cells. # = $p < 0.05$ (Student's t test), as compared to cells treated with CDDP only. § = $p < 0.05$ (Student's t test), as compared to cells treated with PN only. See also Figures S5D–S5H.

(D) Combined effects of PDXK depletion and pyridoxine (PN) administration on stress-induced cell death. PI⁺ = dead cells; PI⁻ DiOC₆(3)^{low} = dying cells. Mean \pm SEM (n = 3). * = $p < 0.05$ (Student's t test), as compared to untreated siUNR-transfected cells. # = $p < 0.05$ (Student's t test), as compared to siUNR-transfected cells treated with the same stress inducer. n.s. = non-significant (Student's t test), as compared to siPDXK-transfected cells treated with the same stress inducer. See also Figure S3D.

high PDXK expression was found in a second cohort of patients with NSCLC who underwent surgery without adjuvant chemotherapy (Table 1; Figure 6C).

There was no inter-individual correlation between PDXK expression in neoplastic lesions and in adjacent normal tissues. However, PDXK protein levels were higher in tumor cells than in their normal counterparts (Figures S6C and S6D). The protein levels of PDXK in the tumor, as quantified by immunohistochemistry and software-assisted image analysis, did not correlate with the amounts of PDXK mRNA, as determined by gene expression profiling (Figure S6E). This suggests that PDXK expression is subjected to a consistent degree of post-translational control. PDXK protein levels had no impact on the survival of patients with NSCLC, and the same held true for other hits from our screen, including ALDH7A1, ALK, BCL-X_L, and WSB2, as deter-

mined by systematic immunohistochemistry (Figures S7A–S7C). Altogether, these results demonstrate that PDXK expression levels constitute a biomarker for risk stratification among patients with NSCLC.

DISCUSSION

In this work, we undertook a near-to-saturating genome-wide siRNA screen to identify novel modulators of the cellular response to CDDP. Driven by the characteristics of the siRNA library that we employed (including four siRNAs per gene product that were predicted, but not guaranteed, to function), we deliberately chose to minimize false-negative results, at the cost of missing potential interesting candidates. Still, this approach and multiple rounds of validation allowed us to

Table 1. Patient Characteristics

Patients with NSCLC: Institut Mutualiste Montsouris (Paris, France)	
Age (years) ^b	63 (41–85)
Follow-up (years) ^{b,c}	4.72
Adjuvant chemotherapy ^a	
No	55 (48.3)
Yes	59 (51.7)
Histology ^a	
ADC	53 (46.5)
SCC	47 (41.2)
Other	14 (12.3)
Stage ^a	
I	50 (47.2)
II	25 (23.6)
III	31 (29.2)
Sex ^a	
F	32 (28.1)
M	82 (71.9)
Smoking status ^a	
Current	44 (38.9)
Former	62 (54.9)
Never	7 (6.2)
Patients with NSCLC: MD Anderson Cancer Center (Houston, TX, USA)	
Age (years) ^b	67 (41–90)
Follow-up (years) ^b	6.27
Adjuvant chemotherapy ^a	
No	218 (100)
Yes	0 (0)
Histology ^a	
ADC	143 (65.6)
SCC	75 (34.4)
Stage ^a	
I	165 (75.7)
II	41 (18.8)
III	12 (5.5)
Sex ^a	
F	118 (54.1)
M	100 (45.9)
Smoking status ^a	
Current	87 (39.9)
Former	103 (47.3)
Never	28 (12.8)

See also Figures S6 and S7.
 ADC, adenocarcinoma; NSCLC, non-small cell lung cancer; SCC, squamous cell carcinoma.
^aAbsolute number (percentage).
^bMedian (range).
^cDFS data were available for 111 patients, *PDXK* mRNA expression data for 109 patients.

identify 85 CRMs, encompassing known apoptosis regulators (negative: MCL1, BCL2L1, TFF1; positive: APAF1) (Bossenmeyer-Pourie et al., 2002; Kroemer et al., 2007), pro-survival proteins (IL6R), as well as multiple proteins involved in intermediate metabolism (homogentisate 1,2-dioxygenase, HGD; high density lipoprotein binding protein, HDLBP; fructosamine-3-kinase-related protein, FN3KRP; COX subunits). The majority of our 85 hits had cytoprotective properties, meaning that their knockdown or their pharmacologic inhibition enhanced CDDP-induced killing. On theoretical grounds, these cytoprotective proteins may constitute novel targets for chemosensitization. Combinatorial analyses suggest that dual interventions on at least two among these gene products may have synergistic effects. Such single- or dual-hit synthetic lethal effects require further exploration as well as biological and pharmacological validation.

The knockdown of PDXK consistently reduced the cytotoxic activity of CDDP. In line with these observations, we found that the exogenous administration of PN (a cell-permeable B6 vitamers) sensitized NSCLC cells to CDDP (in vitro and in vivo). PN-mediated sensitization relied on the presence of PDXK, occurred independently of caspases, and correlated with a bioenergetic and redox catastrophe featuring an abrupt decrease in the intracellular levels of reduced glutathione.

Importantly, we found that PN aggravates, in a PDXK-dependent fashion, the lethal response of cancer cells to a wide range of chemotherapeutics as well as to chemotherapy-unrelated stress conditions, including hyperthermia, ionizing irradiation, hypoxia, respiratory chain inhibition, and nutrient depletion. Thus, the vitamin B6 metabolism appears to regulate stress management in a rather general fashion. This is not surprising given that PLP constitutes the prosthetic group of more than 4% of all enzymes, many of which can influence stress-relevant metabolic circuitries such as those controlling the redox balance (Percedani and Peracchi, 2003). These observations imply that PN renders cancer cells more sensitive to chemical and physical stress via a general, multipronged effect on intermediate metabolism rather than by targeting a single enzymatic activity.

Driven by our pre-clinical results, we quantified (by immunohistochemistry) the expression level of PDXK in specimens from two independent series of patients with NSCLC. Reduced PDXK expression negatively influenced disease-free and overall survival in patients with NSCLC, irrespective of whether they received adjuvant chemotherapy or not, de facto constituting a prognostic biomarker. Intriguingly, circulating vitamin B6 levels negatively correlate with the risk of developing clinically manifest NSCLC (Johansson et al., 2010) and other highly prevalent malignancies including ovarian (Harris et al., 2011) and colorectal cancer (Larsson et al., 2010). Thus, pyridoxine, PDXK, and/or perhaps hitherto unexplored PLP-dependent enzymatic activities may have a profound impact on cancer biology that warrants further investigation.

In conclusion, this study outlines a systems biology strategy for the identification of novel cell death regulators, leading to the discovery of a biomarker for risk stratification in NSCLC. It is our hope that these efforts as well as complementary approaches undertaken by other laboratories will pave the way to an ever more refined stratification of cancer patients and

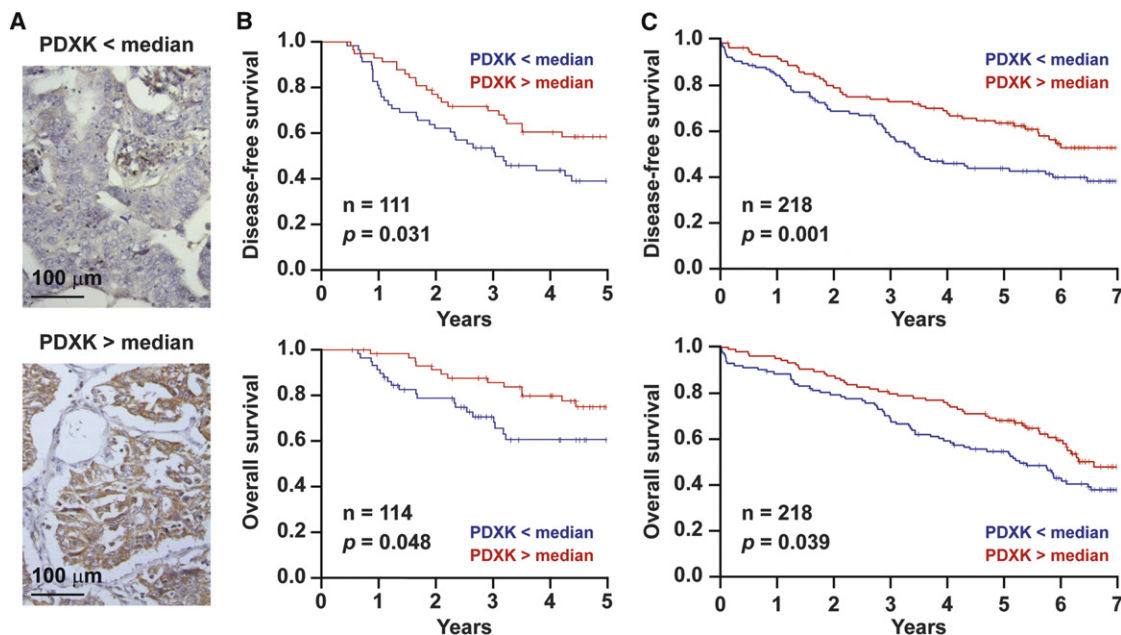


Figure 6. Prognostic Value of PDXK in Patients with NSCLC

(A) Immunohistochemical detection of PDXK levels in biopsies from patients with NSCLC. Bars indicate picture scale. See also Figure S6. (B and C) Kaplan-Meier curves for DFS and OS, in two distinct cohorts of 114 (B) and 218 (C) patients with NSCLC, upon stratification of patients according to median PDXK expression. p values (log-rank test) are depicted. Please note that, in (B), information on DFS was available for 111 patients only. See also Figure S7.

hence to an increasingly sophisticated or “personalized” follow-up, treatment and cure.

EXPERIMENTAL PROCEDURES

Unless otherwise specified, all experiments were performed in triplicate and repeated at least twice. Data are reported as means \pm SEM.

Transfections

The genome-wide siRNA library Human Whole Genome siRNA Set Version 1.0 (QIAGEN, Hilden, Germany) was used in this study. The sequences of the siRNAs selected for low-throughput validation analyses, as well as those of other siRNAs that were employed in this study are reported in Table S2. To avoid depleting the siRNA library of selected sequences, siRNAs for validation experiments were purchased as custom molecules from Sigma-Aldrich (St. Louis, Missouri, USA). For low-throughput experiments, (see below for the transfection protocols employed in the siRNA screen), siRNA were transfected in A549 cells with Oligofectamine™ reagent (Invitrogen, Carlsbad, USA), following the manufacturer's instructions. Transfection with a non-targeting siRNA (siUNR) was employed as a negative control condition. Forty-eight hours after transfection, siRNA-mediated target downregulation was assessed by immunoblotting (see Supplemental Information).

Cytofluorometry

To measure apoptosis-related parameters, living cells were co-stained for 30 min at 37°C with 40 nM 3,3'-dihexyloxalocarbocyanine iodide (DiOC₆(3)), from Molecular Probes-Invitrogen, Eugene, Oregon, USA), which quantifies the mitochondrial transmembrane potential ($\Delta\psi_m$), plus 1 μ g/ml propidium iodide (PI), which only accumulates in cells with ruptured plasma membrane (Galluzzi et al., 2007, 2008, 2009). For the quantification of intracellular reduced glutathione (GSH), cells were labeled for 30 min at 37°C with 50 μ M monochlorobimane (MCB, from Molecular Probes-Invitrogen). All cytofluorometric determinations were carried out a FACSCalibur or a FACScan cytofluorometer (BD Biosciences, San Jose, California, USA) equipped with a 70 μ m nozzle.

First line statistical analysis of cytofluorometric results was performed by using the CellQuest software (BD Biosciences), by gating on the events characterized by normal forward scatter and side scatter parameters. Cytofluorometric data were further analyzed with Microsoft Excel (Microsoft Co., Redmond, WA, USA) and statistical significance was assessed by means of two-tailed Student's t test ($p < 0.05$).

Immunofluorescence Microscopy for the Detection of DNA Damage-Related Signaling

Immunofluorescence microscopy determinations of DNA damage-related events were performed as previously described (Vitale et al., 2007, 2008). Briefly, cells were fixed in 4% (w/v) paraformaldehyde in PBS, permeabilized with 0.1% SDS and immunostained with antibodies recognizing phospho-ATM(Ser1981) (mouse monoclonal IgG₁ κ no. 05-740, Upstate, Billerica, Massachusetts, USA) and phospho-H2AX(Ser139) (γ -H2AX, rabbit antiserum no. 4411, Trevigen, Gaithersburg, Maryland, USA). Slides were then incubated with the appropriate Alexa Fluor 488 conjugates (Molecular Probes-Invitrogen) in the presence of 10 μ M Hoechst 33342 (Molecular Probes-Invitrogen) for nuclear counterstaining. Fluorescence images were acquired using an IRE2 microscope equipped with a DC300F camera (both from Leica Microsystems GmbH, Wetzlar, Germany). Image analysis was performed with the open-source software Image J (National Institutes of Health). The percentage of phospho-ATM and γ -H2AX positivity was assessed by scoring cells that exhibited more than 5 and 10 very bright nuclear spots (DNA damage foci), respectively.

Quantification of Intracellular B6 Vitamers

A549 cells were cultured in absence or the presence of 5 mM pyridoxine (PN), pyridoxamine (PM) or pyridoxal-5-phosphate (PLP) for 24 or 48 hr, harvested, washed once in cold PBS, and pelleted at 800 G for 10 min. Supernatants were discarded and pellets were dissolved in 500 μ l of deionized H₂O by vortexing for 1 min followed by sonication for 10 min. Thereafter, lysates were centrifuged at 5,796 G for 10 min and 60 μ l of the resulting supernatant were mixed with an equal volume of trichloroacetic acid (TCA). Upon additional

centrifugation (5,796 G, 10 min), 50 μ l of sample were injected onto the chromatographic column and PLP, PN, PM and pyridoxal (PL) were measured by liquid chromatography with tandem mass spectrometry (LC-MS/MS), as previously described (Johansson et al., 2010; Midttun et al., 2009).

Metabolomic Profiling

The profiling of intracellular metabolites was performed on a RRLC 1260 system coupled to a Quadrupole-Time of Flight (QTOF) 6520 mass spectrometer (Agilent Technologies, Santa Clara, California, USA), equipped with an electrospray source operating in positive ion and full scan mode from 100 to 1000 Da. The gas temperature was set to 250°C with a gas flow of 8 l/min. Capillary voltage was set to 4.0 kV, and the fragmentor to 100 V. Two reference masses were used to maintain mass accuracy throughout the analysis: 121.050873 and 922.009798 Da. Samples (2 μ l) were injected on a 150 \times 2.1 mm, 3.5 μ m Stable Bond AQ column with a 30 \times 2.1 mm, 3.5 μ m Eclipse plus pre-column (Agilent Technologies). The gradient mobile phase consisted of 0.2% (v/v) acetic acid in water (A) and 0.2% (v/v) acetic acid in methanol (B). The initial composition of the mobile phase was 2% of B, followed by an increase up to 95% of B, uniformly distributed across 15 min. The flow rate was set to 0.3 ml/min. Data collection and analysis were performed with the MassHunter software.

Mouse Strains

C57BL/6 (H-2b) and Swiss Nude mice were obtained from Janvier (Le Genest St. Isle, France) and Charles River (Lille, France), respectively. Animals were maintained in pathogen-free conditions, and all experiments were carried out (upon approval by the local ethical committee, CEEA IRCIV / IGR n°26, registered with the French Ministry of Research) in compliance with Directive EU 63/2010 and following the Federation of European Laboratory Animal Science Association (FELASA) guidelines. Six- to 12-week-old mice were used. During the experiments, animals were subjected to an artificial light cycle (12 hr lights on, 12 hr lights off) and allowed food and drink ad libitum.

Tumor Graft Models

In one model, 5 \times 10⁵ Lewis lung carcinoma (LLC) cells were subcutaneously grafted (in 100 μ l sterile PBS) in immunocompetent (C57BL/6) mice. Alternatively, human 5 \times 10⁶ NSCLC H460 cells were subcutaneously xenografted (in 100 μ l sterile PBS) in immunodeficient (Swiss nude) mice. For induction models (LLC and H460 cells), when the tumor surface reached 25–40 mm², 10–20 mice were assigned to one of four different treatment groups: group 1 = 100 μ l intraperitoneal PBS; group 2 = 5 mg/kg intraperitoneal cisplatin (CDDP) in 100 μ l PBS; group 3 = 170 mg/kg intratumoral PN in 100 μ l PBS; group 4 = 5 mg/kg intraperitoneal CDDP in 100 μ l PBS + 170 mg/kg intratumoral PN in 100 μ l PBS. For regression studies (LLC cells), tumors were allowed to reach a surface of 75–100 mm², then 10–20 mice were assigned to one of four different treatment groups: group 1 = 100 μ l intraperitoneal PBS; group 2 = 25 mg/kg intraperitoneal CDDP in 100 μ l PBS; group 3 = 170 mg/kg intratumoral PN in 100 μ l PBS; group 4 = 25 mg/kg intraperitoneal CDDP in 100 μ l PBS + 170 mg/kg intratumoral PN in 100 μ l PBS. In all cases, treatments were administered three times a week (days 1, 3, and 5; day 8 = day 1), tumor size was routinely monitored by means of a standard caliper and tumor volume was extrapolated as previously described (Streit et al., 1999). Animals bearing tumors that exceeded 20%–25% of total body mass or that exhibited large necrotic lesions were sacrificed. Statistical significance was evaluated by two-way ANOVA.

Patients

Tumors resected from 114 patients with NSCLC from the Institut Mutualiste Montsouris (Paris, France) were fixed in neutral buffered 10% formalin solution and paraffin-embedded. Inclusion criteria were: (1) histologic diagnosis of NSCLC, and (2) complete tumor resection. These biopsy specimens were collected in the context of the CHEMOPREVENTION initiative (an EU funded research collaboration aimed at improving cancer treatment by obtaining increased knowledge on mechanisms of chemotherapy resistance) between 2002 and 2006. Tumor biopsies from 218 patients with NSCLC who never received adjuvant chemotherapy were collected at the MD Anderson Cancer Center (Houston, Texas, USA) in the form of tissue microarrays. An informed written consent

was always obtained from patients, according to the local ethical committee. The main patients' characteristics (i.e., age, sex, tumor histology, follow-up, administration of adjuvant chemotherapy, and other) are summarized in Table 1.

The full set of experimental procedures and statistical methods can be found online as Supplemental Information.

SUPPLEMENTAL INFORMATION

Supplemental Information includes Extended Experimental Procedures, seven figures, and five tables and can be found with this article online at <http://dx.doi.org/10.1016/j.celrep.2012.06.017>.

LICENSING INFORMATION

This is an open-access article distributed under the terms of the Creative Commons Attribution-NonCommercial-No Derivative Works 3.0 Unported License (CC-BY-NC-ND; <http://creativecommons.org/licenses/by-nc-nd/3.0/legalcode>).

ACKNOWLEDGMENTS

Dr. Fabienne Dufour is thanked for her assistance in tissue and clinical data collection. L.G., T.E., and S.S. are funded by Apo-Sys. D.C.G. receives a Lypotoxicity grant from the Austrian FWF. M.N-S. is funded by Junta de Extremadura (Spain). F.M. is grateful to the Austrian FWF (grants LIPOTOX, P23490-B12, P24381-B20, DK MCD W 1226-B18) and to the European Commission (grant Apo-Sys). A.H.B. received financial support from the Association pour la Recherche sur le Cancer (ARC). G.K. is supported by the Ligue Nationale contre le Cancer (Equipe labellisée), Agence Nationale pour la Recherche (ANR), European Commission (Active p53, Apo-Sys, Artforce, ChemoRes, ApopTrain), Fondation pour la Recherche Médicale (FRM), Institut National du Cancer (INCa), Cancéropôle Ile-de-France, AXA Research Fund, and the Labex Immuno-Oncology.

L.G. supervised the project, designed and performed experiments, analyzed data and wrote the paper; L.S., I.V., K.A.O., G.P., T.E., O.M., H.Z., E.C., and M.C. designed and performed experiments; I.M., J.M., G.K., D.C.G., M.S., F.S., O.K., S.S., M.T., E.M., A.C., S.A., M.J., K.C., C.P., M.M., F.P., N.T., T.M.R., N.A., N.M., T.R., P.F., A.R., N.D., N.J., A.C.N., S.M., I.C., D.D., P.B.M., and P.M.U. performed experiments; A.G., E.V., M.N.S., H.R., F.C., C.P., N.S., P.H., V.L., P.D., and E.B. analyzed data and performed bioinformatic studies; B.B., C.B., and M.A. gathered clinical data; P.V., P.G., S.G., and P.P. examined patients and collected clinical samples; K.K., F.M., J.T., C.S.F., L.Z., and A.H.B. designed experiments; I.I.W. and J.C.S. examined patients and directed clinical studies; G.K. designed experiments, wrote the paper, and directed biologic studies.

Received: May 27, 2012

Revised: June 13, 2012

Accepted: June 22, 2012

Published online: July 26, 2012

REFERENCES

- Alavian, K.N., Li, H., Collis, L., Bonanni, L., Zeng, L., Sacchetti, S., Lazrove, E., Nabili, P., Flaherty, B., Graham, M., et al. (2011). Bcl-xL regulates metabolic efficiency of neurons through interaction with the mitochondrial F1FO ATP synthase. *Nat. Cell Biol.* 13, 1224–1233.
- Anastasiou, D., Poulgiannis, G., Asara, J.M., Boxer, M.B., Jiang, J.K., Shen, M., Bellinger, G., Sasaki, A.T., Locasale, J.W., Auld, D.S., et al. (2011). Inhibition of pyruvate kinase M2 by reactive oxygen species contributes to cellular antioxidant responses. *Science* 334, 1278–1283.
- Atkinson, D.E. (1968). The energy charge of the adenylate pool as a regulatory parameter. Interaction with feedback modifiers. *Biochemistry* 7, 4030–4034.
- Bossenmeyer-Pourié, C., Kannan, R., Ribieras, S., Wendling, C., Stoll, I., Thim, L., Tomasetto, C., and Rio, M.C. (2002). The trefoil factor 1 participates in

- gastrointestinal cell differentiation by delaying G1-S phase transition and reducing apoptosis. *J. Cell Biol.* 157, 761–770.
- Brown, C.J., Lain, S., Verma, C.S., Fersht, A.R., and Lane, D.P. (2009). Awakening guardian angels: drugging the p53 pathway. *Nat. Rev. Cancer* 9, 862–873.
- Buchakjian, M.R., and Kornbluth, S. (2010). The engine driving the ship: metabolic steering of cell proliferation and death. *Nat. Rev. Mol. Cell Biol.* 11, 715–727.
- Castedo, M., Coquelle, A., Vivet, S., Vitale, I., Kauffmann, A., Dessen, P., Pequignot, M.O., Casares, N., Valent, A., Mouhamad, S., et al. (2006). Apoptosis regulation in tetraploid cancer cells. *EMBO J.* 25, 2584–2595.
- Cosaert, J., and Quoix, E. (2002). Platinum drugs in the treatment of non-small-cell lung cancer. *Br. J. Cancer* 87, 825–833.
- de La Motte Rouge, T., Galluzzi, L., Olaussen, K.A., Zermati, Y., Tasdemir, E., Robert, T., Ripoche, H., Lazar, V., Dessen, P., Harper, F., et al. (2007). A novel epidermal growth factor receptor inhibitor promotes apoptosis in non-small cell lung cancer cells resistant to erlotinib. *Cancer Res.* 67, 6253–6262.
- Galluzzi, L., Zamzami, N., de La Motte Rouge, T., Lemaire, C., Brenner, C., and Kroemer, G. (2007). Methods for the assessment of mitochondrial membrane permeabilization in apoptosis. *Apoptosis* 12, 803–813.
- Galluzzi, L., Vitale, I., Kepp, O., S  ror, C., Hangen, E., Perfettini, J.L., Modjtahedi, N., and Kroemer, G. (2008). Methods to dissect mitochondrial membrane permeabilization in the course of apoptosis. *Methods Enzymol.* 442, 355–374.
- Galluzzi, L., Aaronson, S.A., Abrams, J., Alnemri, E.S., Andrews, D.W., Baehrecke, E.H., Bazan, N.G., Blagosklonny, M.V., Blomgren, K., Borner, C., et al. (2009). Guidelines for the use and interpretation of assays for monitoring cell death in higher eukaryotes. *Cell Death Differ.* 16, 1093–1107.
- Galluzzi, L., Morselli, E., Vitale, I., Kepp, O., Senovilla, L., Criollo, A., Servant, N., Paccard, C., Hup  , P., Robert, T., et al. (2010). miR-181a and miR-630 regulate cisplatin-induced cancer cell death. *Cancer Res.* 70, 1793–1803.
- Gil, J., and Peters, G. (2006). Regulation of the INK4b-ARF-INK4a tumour suppressor locus: all for one or one for all. *Nat. Rev. Mol. Cell Biol.* 7, 667–677.
- Gyrd-Hansen, M., and Meier, P. (2010). IAPs: from caspase inhibitors to modulators of NF-  b, inflammation and cancer. *Nat. Rev. Cancer* 10, 561–574.
- Hanahan, D., and Weinberg, R.A. (2000). The hallmarks of cancer. *Cell* 100, 57–70.
- Hanahan, D., and Weinberg, R.A. (2011). Hallmarks of cancer: the next generation. *Cell* 144, 646–674.
- Harris, H.R., Cramer, D.W., Vitonis, A.F., Depari, M., and Terry, K.L. (2011). Folate, vitamin B(6), vitamin B(12), methionine and alcohol intake in relation to ovarian cancer risk. *Int. J. Cancer* 131, E518–E529.
- Iwahara, T., Fujimoto, J., Wen, D., Cupples, R., Bucay, N., Arakawa, T., Mori, S., Ratzkin, B., and Yamamoto, T. (1997). Molecular characterization of ALK, a receptor tyrosine kinase expressed specifically in the nervous system. *Oncogene* 14, 439–449.
- Jemal, A., Thun, M.J., Ries, L.A., Howe, H.L., Weir, H.K., Center, M.M., Ward, E., Wu, X.C., Ehemann, C., Anderson, R., et al. (2008). Annual report to the nation on the status of cancer, 1975–2005, featuring trends in lung cancer, tobacco use, and tobacco control. *J. Natl. Cancer Inst.* 100, 1672–1694.
- Johansson, M., Relton, C., Ueland, P.M., Vollset, S.E., Midttun, O., Nyg  rd, O., Slimani, N., Boffetta, P., Jenab, M., Clavel-Chapelon, F., et al. (2010). Serum B vitamin levels and risk of lung cancer. *JAMA* 303, 2377–2385.
- Kroemer, G., and Pouyssegur, J. (2008). Tumor cell metabolism: cancer’s Achilles’ heel. *Cancer Cell* 13, 472–482.
- Kroemer, G., Galluzzi, L., and Brenner, C. (2007). Mitochondrial membrane permeabilization in cell death. *Physiol. Rev.* 87, 99–163.
- Larsson, S.C., Orsini, N., and Wolk, A. (2010). Vitamin B6 and risk of colorectal cancer: a meta-analysis of prospective studies. *JAMA* 303, 1077–1083.
- Lee, H.S., Moon, B.J., Choi, S.Y., and Kwon, O.S. (2000). Human pyridoxal kinase: overexpression and properties of the recombinant enzyme. *Mol. Cells* 10, 452–459.
- Lodi, A., and Ronen, S.M. (2011). Magnetic resonance spectroscopy detectable metabolomic fingerprint of response to antineoplastic treatment. *PLoS ONE* 6, e26155.
- Midttun, O., Hustad, S., and Ueland, P.M. (2009). Quantitative profiling of biomarkers related to B-vitamin status, tryptophan metabolism and inflammation in human plasma by liquid chromatography/tandem mass spectrometry. *Rapid Commun. Mass Spectrom.* 23, 1371–1379.
- Morris, S.W., Kirstein, M.N., Valentine, M.B., Dittmer, K.G., Shapiro, D.N., Saltman, D.L., and Look, A.T. (1994). Fusion of a kinase gene, ALK, to a nucleolar protein gene, NPM, in non-Hodgkin’s lymphoma. *Science* 263, 1281–1284.
- Ni Chonghaile, T., Sarosiek, K.A., Vo, T.T., Ryan, J.A., Tammareddi, A., Moore, Vdel.G., Deng, J., Anderson, K.C., Richardson, P., Tai, Y.T., et al. (2011). Pretreatment mitochondrial priming correlates with clinical response to cytotoxic chemotherapy. *Science* 334, 1129–1133.
- Percudani, R., and Peracchi, A. (2003). A genomic overview of pyridoxal-phosphate-dependent enzymes. *EMBO Rep.* 4, 850–854.
- Previati, M., Lanzoni, I., Corbacella, E., Magosso, S., Guarani, V., Martini, A., and Capitani, S. (2006). Cisplatin-induced apoptosis in human promyelocytic leukemia cells. *Int. J. Mol. Med.* 18, 511–516.
- Rikova, K., Guo, A., Zeng, Q., Possemato, A., Yu, J., Haack, H., Nardone, J., Lee, K., Reeves, C., Li, Y., et al. (2007). Global survey of phosphotyrosine signaling identifies oncogenic kinases in lung cancer. *Cell* 131, 1190–1203.
- Seth, R., Yang, C., Kaushal, V., Shah, S.V., and Kaushal, G.P. (2005). p53-dependent caspase-2 activation in mitochondrial release of apoptosis-inducing factor and its role in renal tubular epithelial cell injury. *J. Biol. Chem.* 280, 31230–31239.
- S  ve, P., and Dumontet, C. (2005). Chemoresistance in non-small cell lung cancer. *Curr. Med. Chem. Anticancer Agents* 5, 73–88.
- Stoica, G.E., Kuo, A., Powers, C., Bowden, E.T., Sale, E.B., Riegel, A.T., and Wellstein, A. (2002). Midkine binds to anaplastic lymphoma kinase (ALK) and acts as a growth factor for different cell types. *J. Biol. Chem.* 277, 35990–35998.
- Streit, M., Riccardi, L., Velasco, P., Brown, L.F., Hawthornt, T., Bornstein, P., and Detmar, M. (1999). Thrombospondin-2: a potent endogenous inhibitor of tumor growth and angiogenesis. *Proc. Natl. Acad. Sci. USA* 96, 14888–14893.
- Tajeddine, N., Galluzzi, L., Kepp, O., Hangen, E., Morselli, E., Senovilla, L., Araujo, N., Pinna, G., Larochette, N., Zamzami, N., et al. (2008). Hierarchical involvement of Bak, VDAC1 and Bax in cisplatin-induced cell death. *Oncogene* 27, 4221–4232.
- Tesniere, A., Schlemmer, F., Boige, V., Kepp, O., Martins, I., Ghiringhelli, F., Aymeric, L., Michaud, M., Apetoh, L., Barault, L., et al. (2010). Immunogenic death of colon cancer cells treated with oxaliplatin. *Oncogene* 29, 482–491.
- Vitale, I., Galluzzi, L., Vivet, S., Nanty, L., Dessen, P., Senovilla, L., Olaussen, K.A., Lazar, V., Prudhomme, M., Golsteyn, R.M., et al. (2007). Inhibition of Chk1 kills tetraploid tumor cells through a p53-dependent pathway. *PLoS ONE* 2, e1337.
- Vitale, I., Senovilla, L., Galluzzi, L., Criollo, A., Vivet, S., Castedo, M., and Kroemer, G. (2008). Chk1 inhibition activates p53 through p38 MAPK in tetraploid cancer cells. *Cell Cycle* 7, 1956–1961.
- Vousden, K.H., and Ryan, K.M. (2009). p53 and metabolism. *Nat. Rev. Cancer* 9, 691–700.
- Ward, P.S., and Thompson, C.B. (2012). Metabolic reprogramming: a cancer hallmark even warburg did not anticipate. *Cancer Cell* 21, 297–308.
- Youle, R.J., and Strasser, A. (2008). The BCL-2 protein family: opposing activities that mediate cell death. *Nat. Rev. Mol. Cell Biol.* 9, 47–59.